Defence Science Journal, Vol. 74, No. 5, September 2024, pp. 763-774, DOI : 10.14429/dsj.74.19593

Impact of Blowing Location on the Aerodynamic Characteristics Over the Delta Wing

Sugandh Gupta[#,*], Sanjeev Kumar[#] and Rakesh Kumar[!]

[#]*Department of Mechanical Engineering, Punjab Engineering College, Chandigarh – 160 012, India*
[!]*Department of Aerospace Engineering, Punjab Engineering College, Chandigarh– 160 012, India*
[*]*E-mail: sugandh.gupta90@gmail.com*

ABSTRACT

The performance of an aircraft can be enhanced by altering the flow field favourably by adopting flow control techniques. The present study deals with the application of the active flow control methods on a sharp-edged delta wing with a wing sweep of 65°. The concept of blowing was employed as an active flow control technique. The blowing technique is applied on the suction surface of the delta wing by varying its location. The various identified locations of the blowing holes are 1.62 %, 3.24 % and 4.86 % of root chord from the leading edge to the centre of the blowing holes. The computation is performed using the commercial software ANSYS Fluent. An unsteady, incompressible Reynolds-averaged Navier–Stokes equation and the shear-stress transport k-ω turbulence model are employed. The angles of attack varied in the range of $0^{\circ}<\alpha<35^{\circ}$ and Reynolds number is 2.64×10^{6} and the jet momentum coefficient is fixed at 0.05. The blowing of air from the injection region enhances the strength of the leading-edge vortices, resulting in a delay in the vortex breakdown. The performance of the delta wing is greatly improved while using the blowing method specifically for the blowing holes located at 3.24 % of root chord from the leading edge compared to without the blowing method.

Keywords: Vortex breakdown; Jet momentum coefficient; Sweep angle; Delta wing; Blowing

NOMENCLATURE

C_L	: Lift coefficient
Λ	: Wing sweep angle
A	: Angle of attack
Cr	: Root chord
Re	: Reynolds number
Cμ	: Jet momentum coefficient
m_j	: Mass flow of jet
V_j	: Velocity of jet
S	: Planform area
Q	: Dynamic pressure
Cp	: Pressure coefficient
x/c	: Ratio of x-location chordwise to the local chord
Y/S	: Ratio of y-location spanwise to the local span of the wing

1. INTRODUCTION

Because of the recent increasing interest in unmanned combat air vehicles, micro air vehicles and unmanned air vehicles, many researchers have focussed on the enhancement of flow structure over slender and non-slender delta wings. The flow topology over a delta wing with the sharp leading edge is shown in Fig. 1. The Aerodynamics of delta wings primarily deals with lift, which consists of potential lift and vortex lift. The vortex lift has a very nonlinear structure and is heavily influenced by the angle of attack. The vortex lift varies directly proportional with the angle of attack until stalling angle of attack. Delta wing aerodynamics are characterised by two leading edge vortices. The response of these vortices during manoeuvring flight is the dominant aspect of the flow. Leading-edge vortex breakdown occurs over the delta wing at crucial angles of attack. The vortex collapse has a negative impact on the delta wing aerodynamics, causing the wing and fin to buffet and the lifting force to degrade. Because vortex disintegration is a severe issue, both active and passive flow control techniques can help.

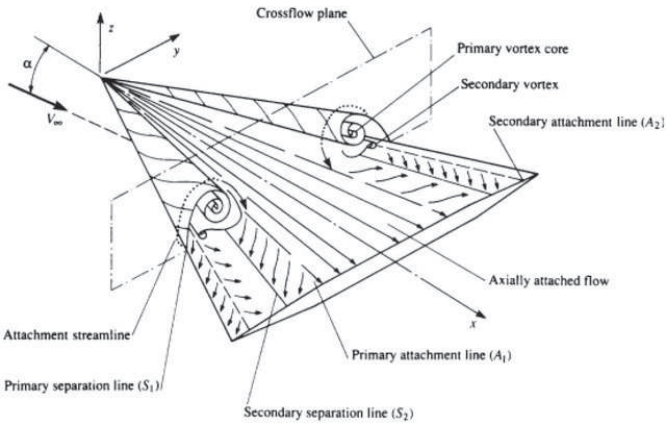

Figure 1. Schematic view of flow over a delta wing with sharp leading edge[1].

Delta wings can be classified on the delta wing's sweep angle. For a delta wing having sweep angle of less than 60°

Received : 06 November 2023, Revised : 23 April 2024
Accepted : 07 June 2024, Online published : 19 September 2024

can be termed as a non-slender delta wing, whereas slender or highly swept delta wings have a sweep angle greater than 65°. The analogy of the leading-edge suction was created by Polhamus[2-3], *et al*. The relation holds true for thin wings with no camber. In addition to this, the strategy applies to sharp-edged delta wings where flow separation is more prone near the leading edge region. Slender delta wings are suitable for high-speed fighter planes. Conversely, in a subsonic flight regime, this wing typically exhibits a low aerodynamic performance. To augment the aerodynamic characteristics, especially at high angles of attack, a lot of research has been performed, employing many devices which include active and passive flow control techniques.

Mitchell,, *et al.* used periodic tangential blowing at the leading edge to control the flow over a slender delta wing, finding that the aerodynamic performance was noticeably improved[4]. In their investigation, Greenblatt,, *et al.* performed an experimental study on a delta wing sweep angle of 60° with DBD plasma actuators with a direction perpendicular to the leading edge and reported a gradual increase in the normal force coefficient at post-stall angles[4]. Numerous kinds of research have been conducted that employed the DBD plasma actuator in controlling the flow[6-10].

Yavuz, *et al.* conducted an experimental study on a delta wing with a sweep angle of 38.7° to examine the flow characteristics of streamlines, velocity pattern and vorticity in the close vicinity of the delta wing surface using the particle image velocimetry based on a laser technique[11]. Yaniktepe and Rockwell experimentally investigated the flow field pattern behaviour over the delta wings with varying leading-edge sweep angles in the close vicinity of the trailing edge on the lambda and diamond planforms[12]. Ol and Gharibexperimentally studied the nature and intensity of the leading-edge shear layer and pair of vortical flow structures inside the shear layer in the crossflow plane over delta wings with a sweep angle of 50° and 65°[13].

Taylor and Gursul performed a wind tunnel test to investigate the effect of the unstable vortex structures and reaction of buffeting phenomenon for a 50° wing sweep delta wing. It was reported that at a small angle of attack, a dual vortex structures system was observed. Also, velocity fluctuations were abrupt near the line of reattachment. Controlling vortex breakdown in the case of slender delta wings is a crucial problem, whereas, for non-slender delta wings, leading-edge vortex breakdown is noted to be gradual[14]. For a delta wing with a sweep angle of 50°, Chen,, *et al.* numerically investigated the impact of the Reynolds number on the vortex flow[15].

Sahin, *et al.* performed the dye visualization and stereoscopic PIV method to investigate the flow behaviour on the 40° wing sweep delta wing and concluded that the location of vortex breakdown mainly depends on the yaw angle[16]. Gursul, *et al.* reviewed many types of flow control devices to regulate the flow control parameters such as leading-edge vortex breakdown or formation, flow separation and attachment[17]. Mitchell, *et al.* investigated how core blowing affected the collapse of the vortex over a slender delta wing[4]. By shifting the vortex collapse site downstream of the root chord by 20 %, they were able to delay the vortex breakdown using this arrangement. Renac, *et al.* used fluidic blowing to try to regulate the vortical flow over a delta wing with a sweep angle of 60° and rounded leading edges[18]. The effect of lateral blowing on the delta wing to regulate vortex breakdown from an extremely low to medium range angle of attack was investigated by Hong, *et al.* They came to the conclusion that the jet momentum coefficient and angle of attack had a notable impact on the strength and location of vortex collapse[19]. From a small to a large angle of attack, Wood and Roberts examined the impact of blowing the air tangentially to the suction surface on a 60° wing sweep delta wing[20].

They demonstrated how managing the main separation allows one to regulate the vortex breakup. In their experiment, Greenwell and Wood modified the flow by utilising the Coanda effect on the leading-edge blowing. It was noticed that the flow was attached at low angles of attack and the phenomenon of vortex formation was absent[21]. Gu, *et al.* conducted research to investigate the influence of the blowing, suction and their combined effect on the rounded leading-edge delta wing[22].

Williams, *et al.* examined how flow structures behaved on a 50° wing sweep delta wing. Their investigation showed an appreciable lift force increase and stall delay[23]. Cui, *et al.* executed the influence of blowing near the forebody over a 60°. wing sweep delta wing[23]. Jiang, *et al.* carried out an experimental investigation on the effects of irregular blowing towards the trailing edge over a delta wing with a sweep angle of 60°[25]. Johari, *et al.* applied the blowing technique at various blowing angles with a spanwise direction[26]. Lamar performed an experiment using an aileron positioned near the trailing edge of a cropped delta wing. This arrangement induced a constant rolling moment[27]. Rao and Campbell investigated the effect of passive flow control techniques such as vortex generators, and leading-edge vortex flaps which can be mounted either on lower or upper surfaces[28].

Smith, *et al.* performed experiments to investigate the flow over slender and non-slender delta wings and compared the strength of the leading-edge vortices and identified the vortex using the Q, $\lambda 2$ and λci criterion[29]. Sedlacek, *et al.* performed an experimental study on a triple and a double delta wing design at high angles of attack and angles of sideslip[30]. It was reported that for high angles of attack, lateral disturbances will be higher. Balogun, *et al.* experimentally studied the flow characteristics on slender delta wings using trailing edge jets mechanism and studied the effect of the jet angle, Reynolds number and angle of attack on the flow behaviour[31].

The present study is mainly concerned with the formation and breakdown of the vortex over the delta wing adopting the active flow control technique to delay the vortex breakdown by shifting the location of the vortex breakdown downstream, towards the trailing edge. The study is conducted using unsteady, incompressible, RANS simulations with the commercial flow solver ANSYS Fluent. In this paper, the aerodynamic characteristics of the delta wing with sweep angle, $\Lambda = 65°$ using three different leading-edge blowing configurations for various angles of attack varying from 0° to 35° are estimated and compared.

Consequently, the study's initial goal was to successfully and consistently collect numerical data on the 65° delta's

aerodynamic performance. These outcomes were then compared with previous numerical and experimental results that have been identified in the literature. After validating the results, the study can be extended to meet the present objectives of the study. To investigate how blowing affects the vortex breakdown process and greatly improves the vortex lift envelope, it will be useful to know the optimum position for spanwise suction for a delta wing for various blowing configurations.

2. METHODOLOGY

The delta wing that did not adopt the flow control technique was selected as a baseline delta wing with a root chord (C_r) of 0.247 m and a sweep angle of 65°, as shown in Fig. 2(a). The other three delta wing configurations utilised the blowing technique with different blowing locations over the suction surface of the delta wing.

The different locations of blowing ports were made on the suction surface of the delta wing located at 1.62 % (blowing configuration (1), 3.24 % (blowing configuration (2) and 4.86 % (blowing configuration (3) of the root chord from the centre of the blowing port to the leading edge as shown in Fig. 2(b), 2(c) and 2(d), respectively. The diameter of each of the blowing holes was 2 mm and a total of 14 blowing holes were located on the suction surface. The distance between the holes from centre to centre was 15 mm.

The first blowing hole was located at a distance of 40 mm from the apex of the delta wing. The flow conditions for the present study are shown in Table 4. The Reynolds Number (Re) based on the mean aerodynamics chord (mac) was 2.64×10^5. The angle of attack (AoA) varied from 0° to 35°. For the non-dimensional jet momentum coefficient C_μ = 0.05, the ratio of the jet velocity to the freestream velocity value is 2.3. The jet momentum coefficient was calculated as:

$$C_\mu = \frac{Q_j V_j}{U_\infty^2 S},$$

Where

Q_j = volumetric flow rate of the jet; V_j = mean velocity of the blowing at leading edge

$\boldsymbol{U}_\infty$ = freestream velocity; S = planform area

2.1 Description of a Validation Model

The model was designed for validation purposes with the following specifications as shown in Table 1.

Once the validation part was over, much attention was required to simulate the model with the key geometrical features, as shown in Table 3. The flow conditions for the present study are shown in Table 4.

Table 1. Design parameters of the delta wing model[32]

Design parameters	Specifications of delta wing
Leading-edge sweep Angle, Λ	65°
Root chord, c_r	0.3 m
Wing span, b	0.2798 m
Wing area, S	0.04197 m
Aspect ratio, AR	1.865
Thickness	0.01 m
Bevel angle	8.5°

Table 2. Test conditions for validation

Flow conditions	Value
Freestream velocity	13 m/s
Dynamic pressure	100 N/m^2
Re_c	2.67×10^5
Temperature	300 K
Atmospheric pressure	1.008×10^5 N/m^2
Angle of attack range	0–35°

Table 3. Delta wing design with/without blowing

Design parameters	Specifications of delta wing
Leading-edge sweep angle, Λ	65°
Root chord, c_r	0.247 m
Wingspan, b	0.230 m
Wing area, S	0.028405 m^2
Aspect ratio, AR	1.862
Thickness	0.015 m
Bevel angle	45°
Blowing locations	1.62 %, 3.24 % & 4.86 % of c_r

Table 4. Flow conditions for the present study

Flow conditions	Value
Freestream velocity	15.6 m/s
Dynamic pressure	148.8 N/m^2
Re_c	2.67×10^5
Temperature	300 K
Atmospheric pressure	1.008×10^5 N/m^2
Angle of attack range	0–35°
Momentum coefficient	0.05

The port side of the delta wing was selected for the present investigation. This is because the flow structure on the port side and starboard side of the delta wing exhibited very little difference in terms of vortex strength. For the 0° angle of attack, the upstream boundary was selected as the velocity inlet and the downstream wall as the pressure outlet. The top and bottom wall was selected as a wall. The left boundary was selected as symmetry and the right boundary as the wall boundary. For the angles of attack other than 0°, velocity inlet boundary conditions were applied for the upstream as well as bottom boundary of the computational domain of the delta wing[35]. Downstream of the delta wing as well as the top boundary of the computational domain was selected as the pressure outlet boundary condition. The upstream boundary was placed at 10 Cr from the apex of the delta wing. The downstream location, top boundary, bottom boundary and left boundary were placed at 20 Cr.

Mass flow inlet boundary conditions were applied at the blowing holes. The grid was generated for the half delta wing along with its domain using the commercial software ANSYS®

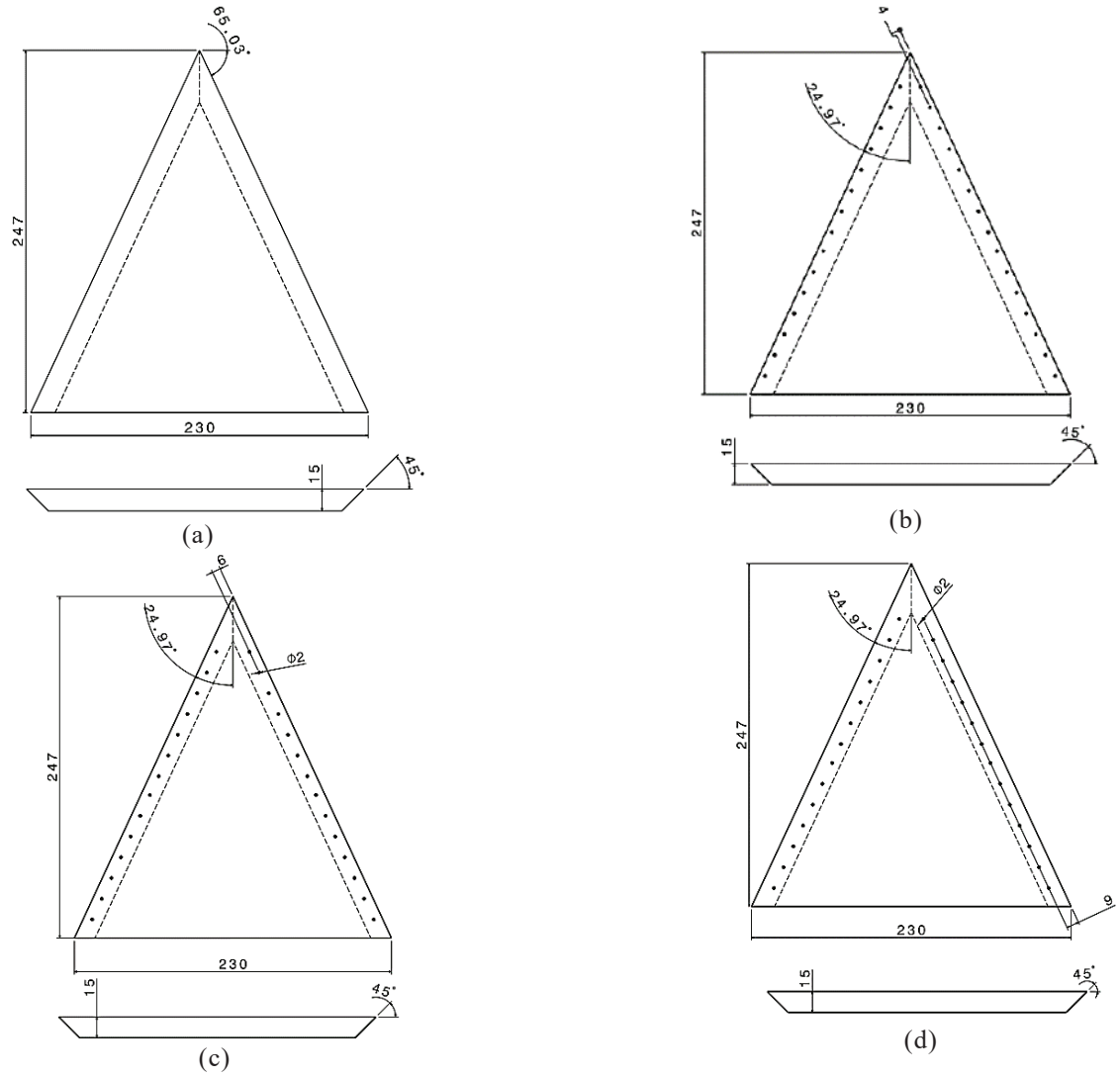

Figure 2. Geometry of the baseline delta wing with different blowing configurations (units in mm): (a) Baseline delta wing; (b) Blowing configuration 1; (c) Blowing configuration 2 and (d) Blowing configuration 3.

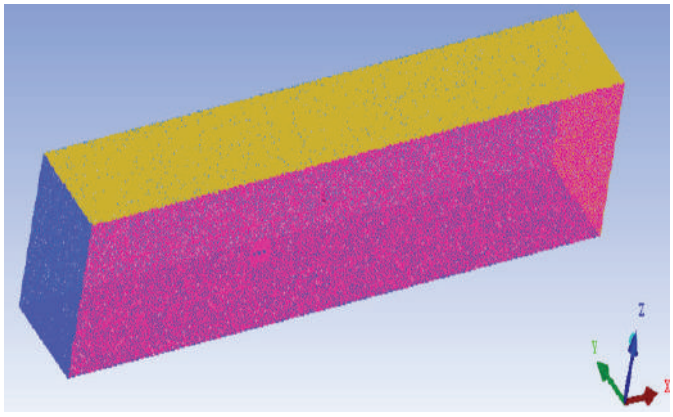

Figure 3. Grid generated inside the computational domain.

ICEM CFD 2021 R2. The mesh was more refined close to the leading edge, trailing edge, the region near the leading-edge vortices and the blowing holes. The grid generated based on maximum $y^+ = 1$ contained 35 million cells. The grid generated inside the domain is shown in Figure 3.

To capture the viscous effects inside the boundary layer, twenty prism layers were included inside the boundary layer.

Table 5. Grid details

Parameter	Value
Grid size (number of cells)	35 million
Grid type	Tetrahedral
Number of prism layers	20
First cell height	10^{-6} m
Growth rate	1.2
Reynold's number	2.64×10^5
Mach number	0.06
Total memory consumed (MB)	2514
Processor type	Intel Xeon
Number of cores	32
RAM (GB)	128
Average CPU time/iteration, s	8

The details of the grid are shown in Table 5. The zoomed view of the grid around the delta wing with the prism layers is shown in Figure 5(a,b). Figure 6 shows the grid on the symmetry plane of the delta wing with configuration 1 and Fig. 7 represents the

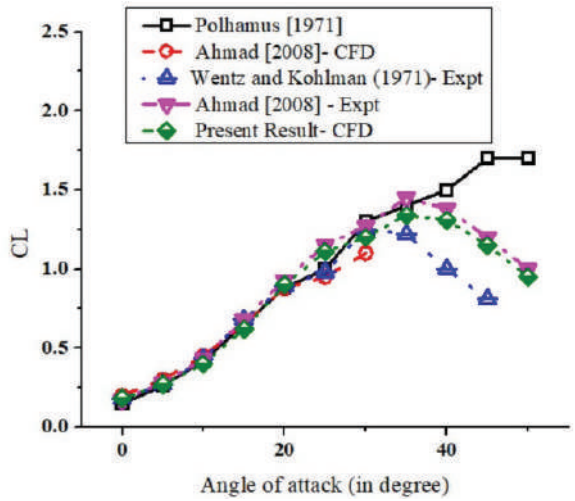

Figure 4. Validation of the lift coefficient (CL) vs. angle of attack (α)[2,31,32].

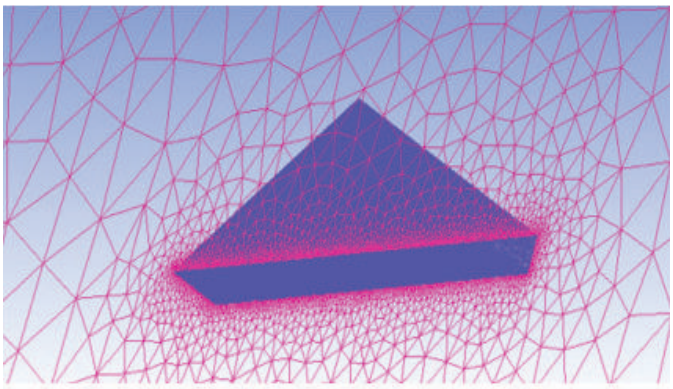

(a)

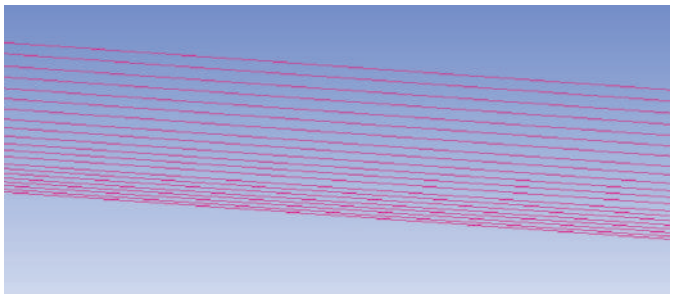

(b)

Figure 5. Zoomed view of the grid around the baseline delta wing. (a) Grid around the baseline delta wing with prism layers on the symmetry plane; and (b) Close-up view of the grid representing the prism layers above the surface of the baseline delta wing.

zoomed view of the surface grid on the suction surface of the delta wing with configuration 1.

ANSYS® FLUENT® 2021 R2 software was employed as a solver to numerically simulate the prescribed problem. In the initial phase, the numerical model was validated using the results available in the literature for the baseline delta wing with the present numerical result, as shown in Fig. 4. The similar boundary conditions and solver set-up were adopted

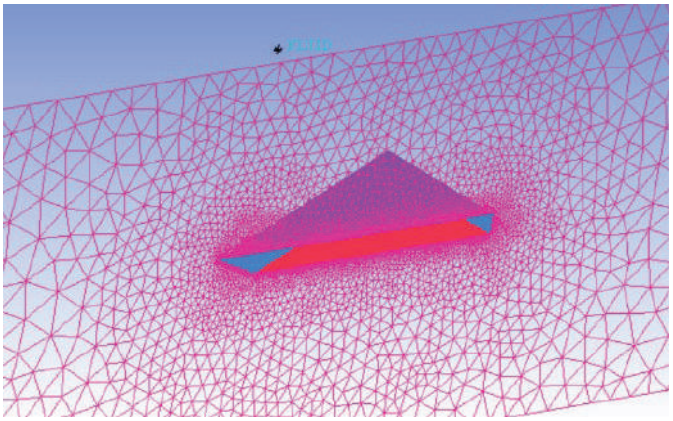

Figure 6. Grid on the symmetry plane of the delta wing with blowing configuration 1.

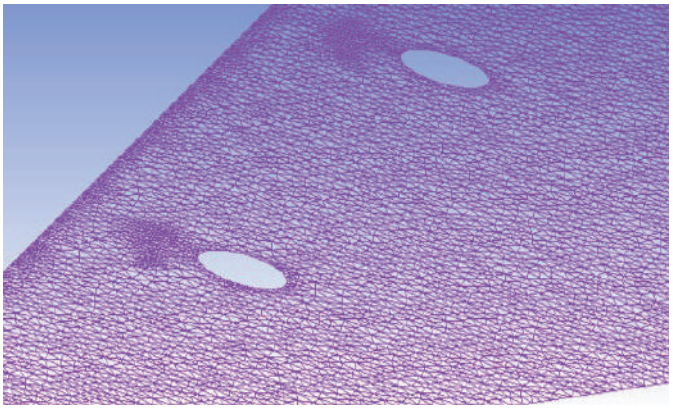

Figure 7. Zoomed view of the surface grid on the suction surface of the delta wing with blowing configuration 1.

for the present study based on delta wings using an active flow control technique.

The three-dimensional unsteady, pressure-based RANS equation and turbulence model adopted as SST-K-omega with both low Reynold's number corrections and curvature corrections was selected for the numerical simulation. The SST-K-omega more accurately predicts the leading-edge vortex breakdown location and its strength[32,34]. Pressure based solver using SIMPLEC (Semi-Implicit Method for Pressure-

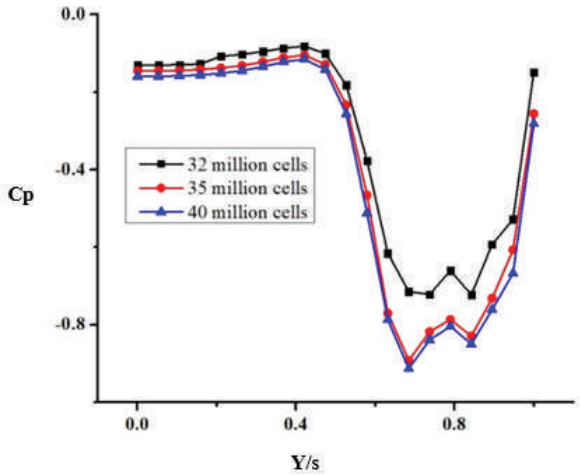

Figure 8. Grid independence test: plot of Cp vs. Y/s at x/c = 0.2.

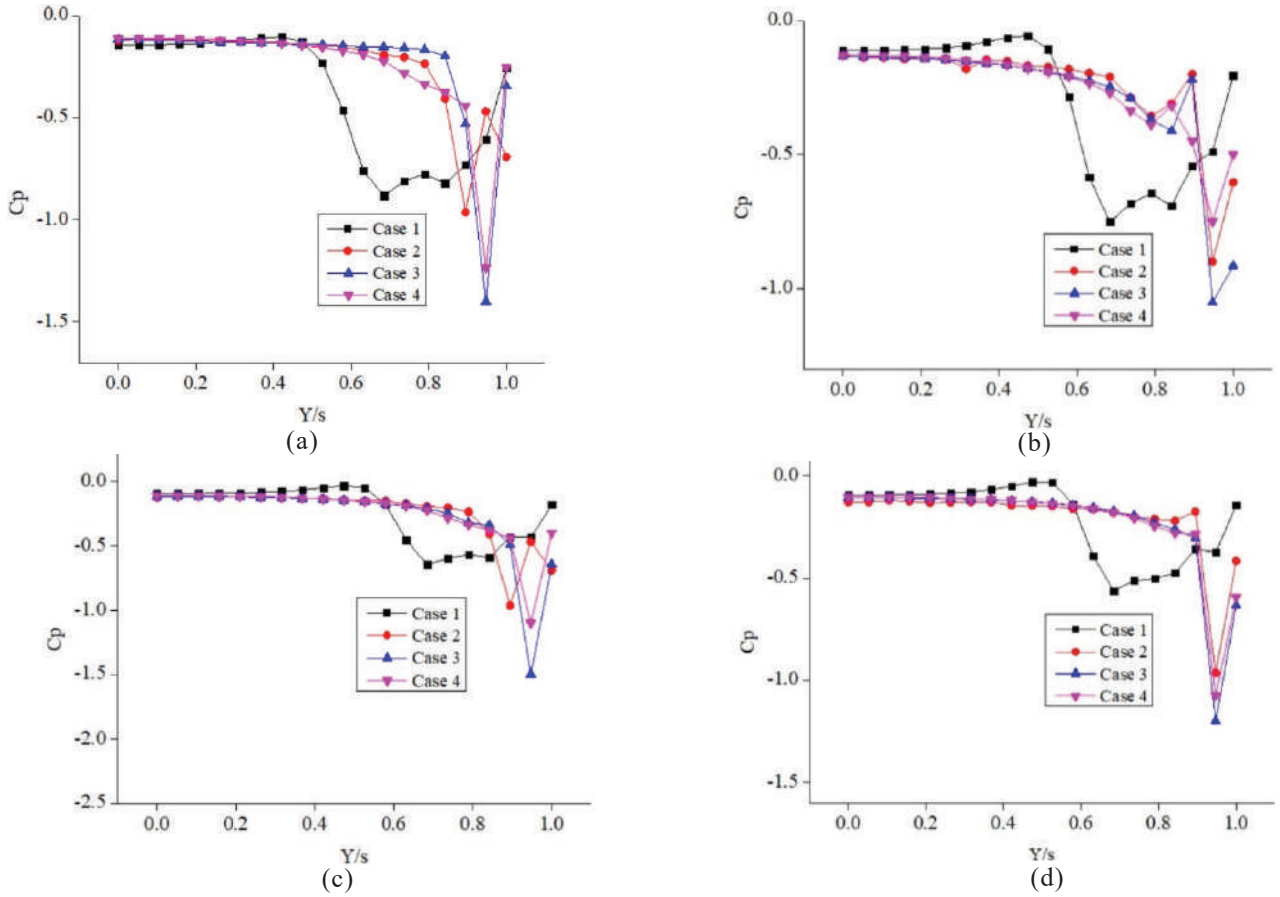

Figure 9. (a) x/c = 0.2; (b) x/c = 0.4; (c) x/c = 0.6; (d) x/c = 0.8. Cp distribution versus Y/s for various x/c at 5° angle of attack.

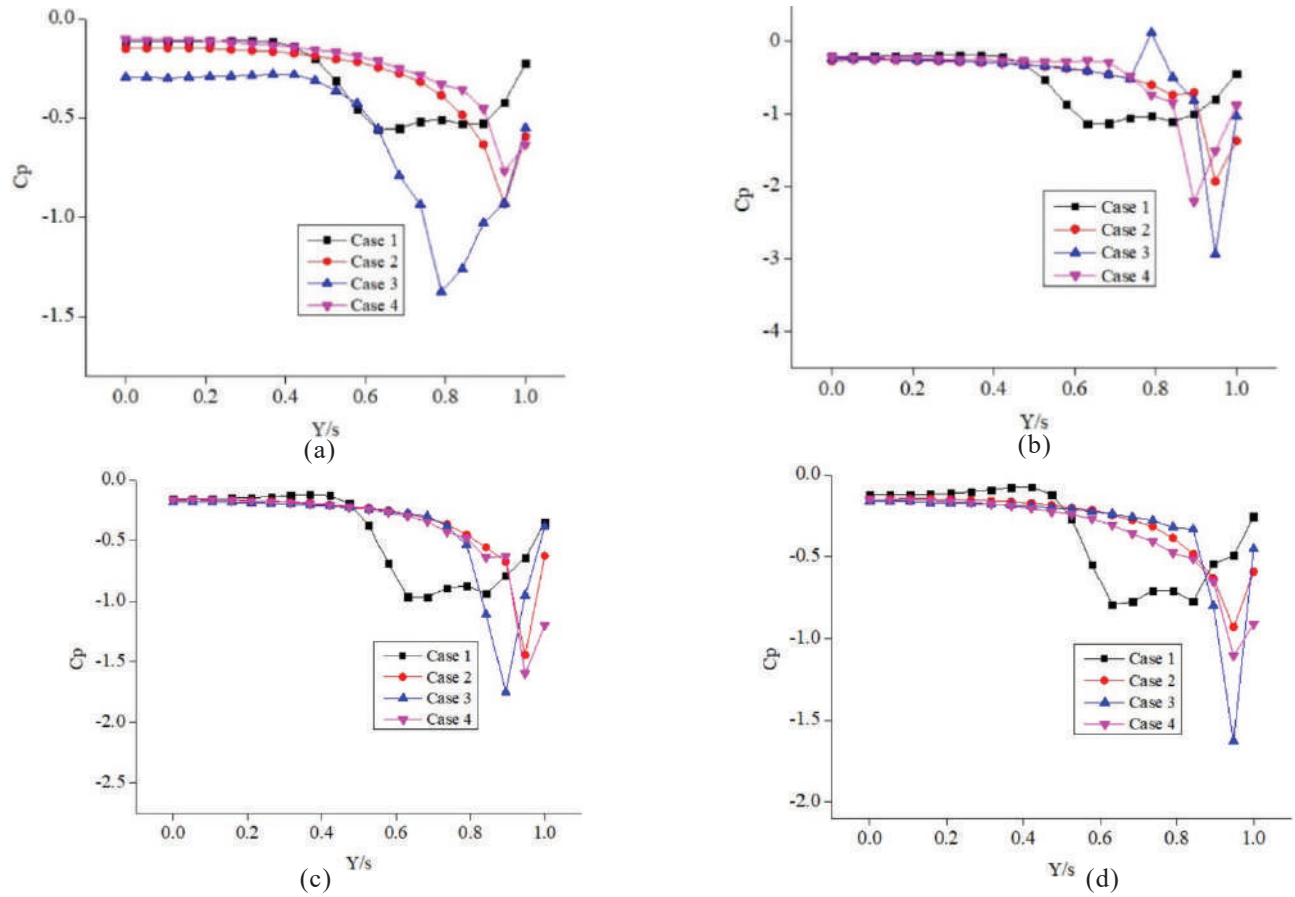

Figure 10. (a) x/c = 0.2; (b) x/c = 0.4; (c) x/c = 0.6; (d) x/c = 0.8. Cp distribution versus Y/s for various x/c at 10° angle of attack.

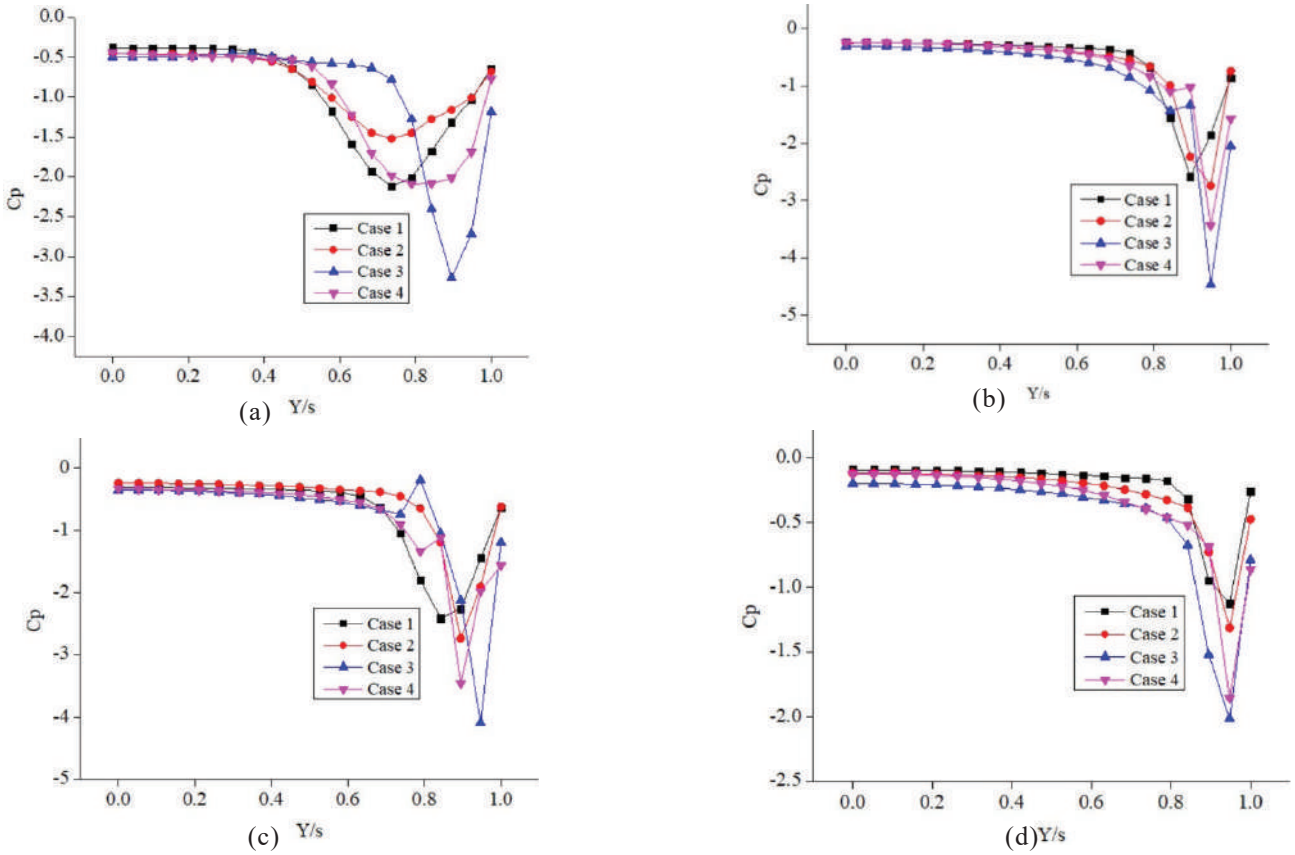

Figure 11. (a) x/c = 0.2; (b) x/c = 0.4; (c) x/c = 0.6; (d) x/c = 0.8. Cp distribution versus Y/s for various x/c at 15° angle of attack.

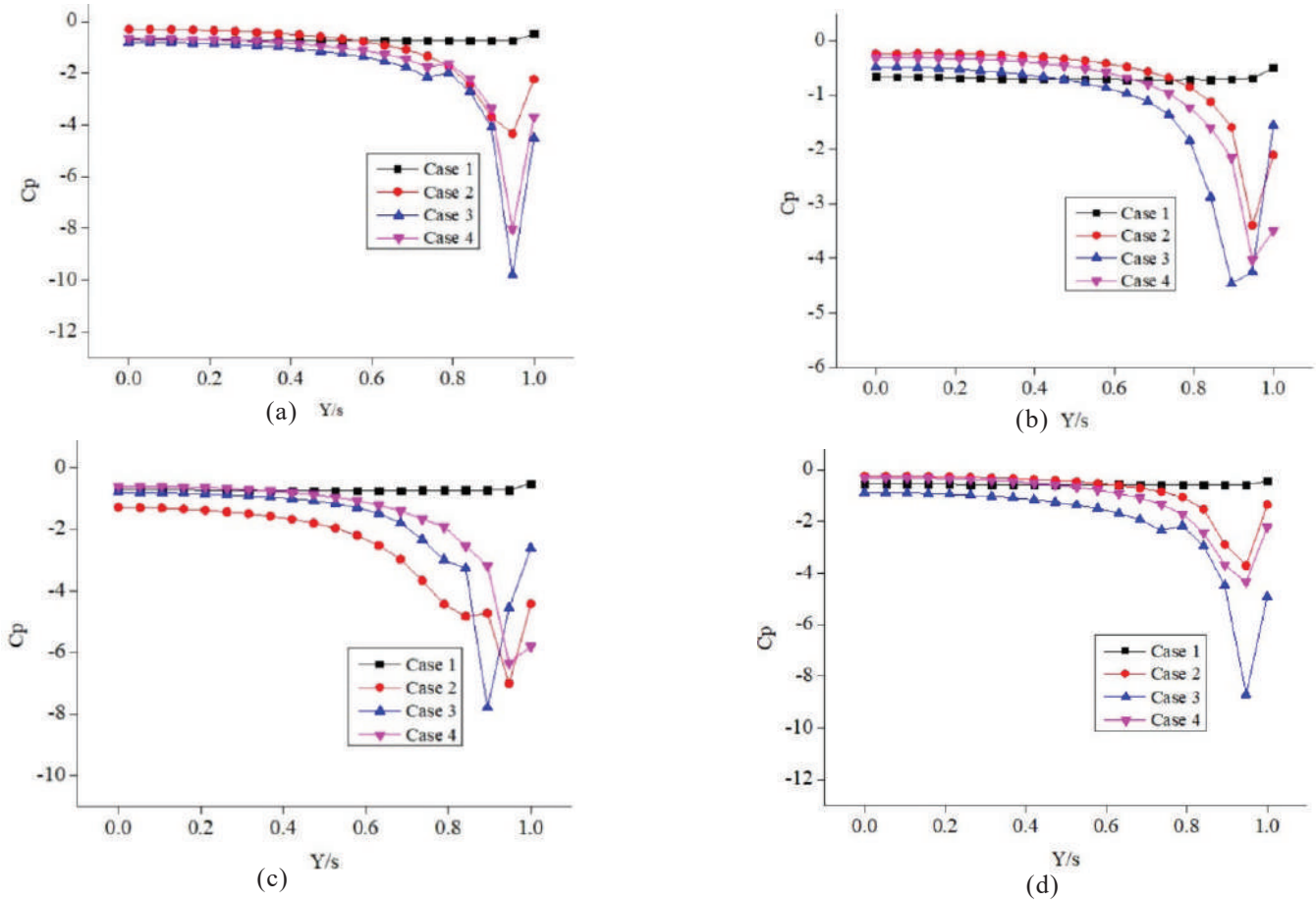

Figure 12. (a) x/c = 0.2; (b) x/c = 0.4; (c) x/c = 0.6; (d) x/c = 0.8. Cp distribution versus Y/s for various x/c at 30° angle of attack.

Linked Equations Consistent) technique is adopted for the coupling of pressure & velocity. For spatial discretization of the computational domain, the cell-based least square was chosen with second-order accuracy. The fixed time-stepping of 0.002s was chosen to capture the flow physics of the leading-edge vortex breakdown[35]. The residual convergence criterion for all the variables was 1×10^{-5}.

3. RESULTS AND DISCUSSION

A grid-independence test was performed to ensure that the computational results do not depend on the sensitivity of the grid size, indicating that the simulation has reached a level of mesh refinement where further grid refinement will not substantially alter the results. Three different grids containing 32 million cells, 35 million cells and 40 million cells were generated around the baseline delta wing to estimate the pressure distribution (C_p) with respect to the non-dimensional distance along the span (Y/s) at a chord-wise distance of 25 % of the root chord, as shown in Fig. 8. Less difference in the results was obtained compared to the simulation based on a grid size of 35 million cells and 40 million cells. Therefore, a grid of 35 million cells was selected for the present case comprising the baseline and blowing configurations of the delta wing.

The different configurations of the delta wings are numerically simulated. The different cases considered are as follows. Case 1: baseline delta wing without any flow control technique, case 2: delta wing with injection ports located at 1.62% of c_r from its centre to the leading edge, case 3: delta wing with injection ports located at 3.24 % of c_r from its centre to the leading edge and case 4: delta wing with injection ports located at 4.86 % of c_r from its centre to the leading edge.

In all cases, the wing sweep angle of the delta wing is fixed at 65°.The pressure coefficient plot versus the local Y/s location at the fixed chord station of x/c ranging from 0.2 to 0.8 with an interval of 0.2 is chosen. The Cp distribution graph for the 5° angle of attack is shown in Fig. 9. From these results, it can be clearly observed that the suction peak for case 3 is relatively higher than the other cases considered. This may be because the stagnant fluid flow at the separation zone interacts with the fluid flow blown on the upper surface, effectively resulting in the momentum transfer, and this mixing phenomenon increases the overall suction. The lift generated for case 3 is higher due to the presence of the higher suction zone. The maximum suction peak is observed for case 3 at x/c = 0.6. As can be clearly analysed based on Fig. 10. C_p for case 3 attains the maximum value at x/c = 0.4 at 10°angle of attack. For x/c = 0.8, the C_p for case 3 is considerably higher than the other cases. This shows that the phenomenon of flow separation is largely restricted and delayed. For a 15° angle of attack, as shown in Fig. 11, the C_p value has a maximum suction at x/c = 0.6. The C_p difference between case 1 and case

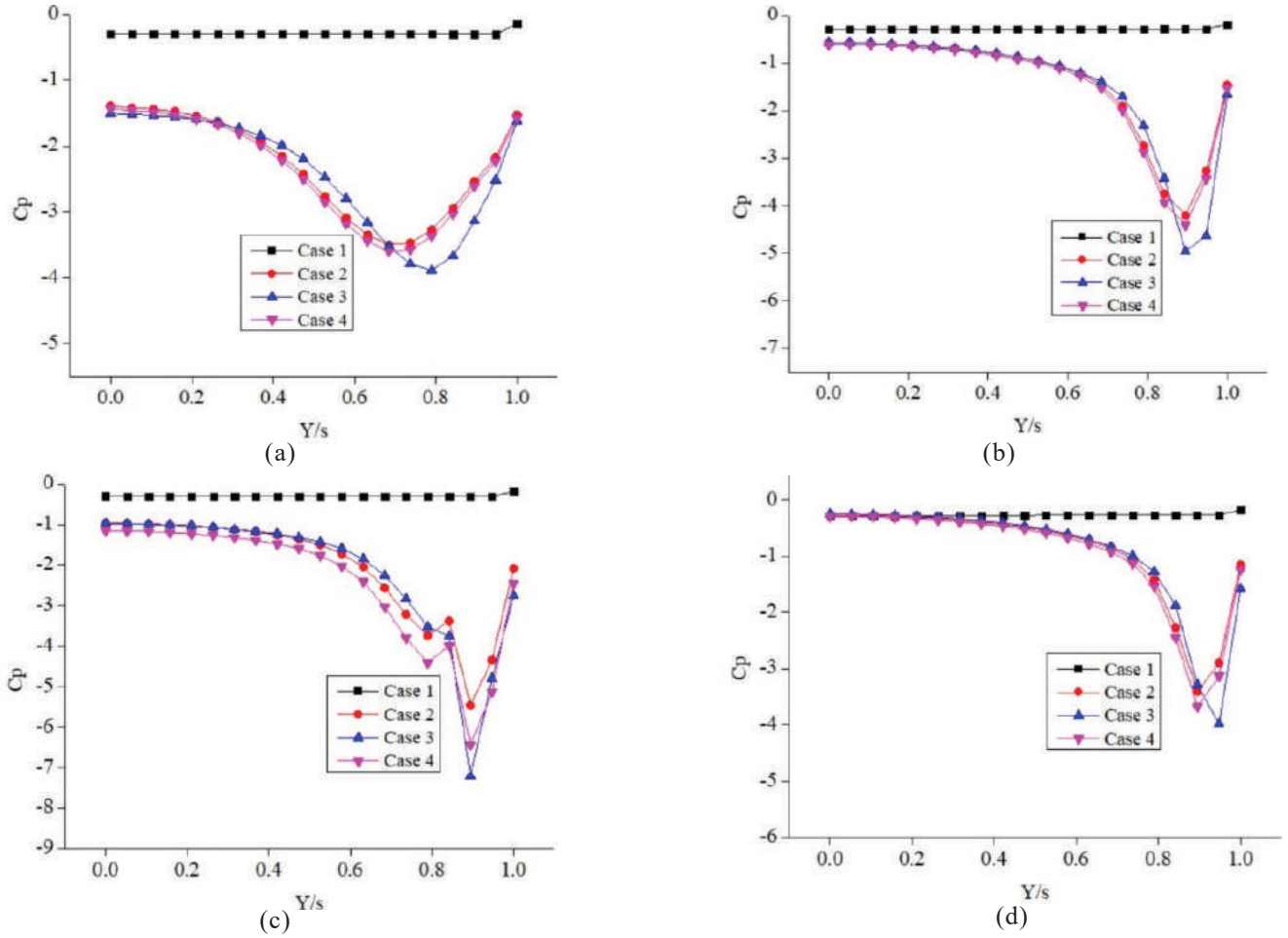

Figure 13. (a) x/c = 0.2; (b) x/c = 0.4; (c) x/c = 0.6; (d) x/c = 0.8. Cp distribution versus Y/s for various x/c at 35° angle of attack.

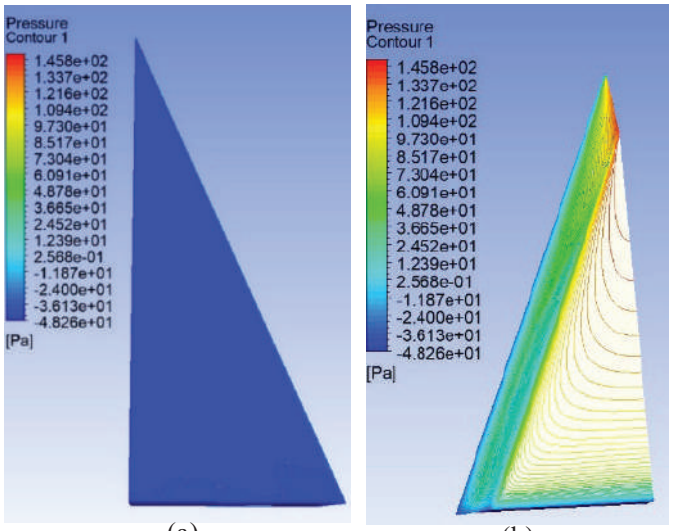

(a) (b)

Figure 14. Pressure contours for the baseline delta wing at α = 35°. (a) Top surface; and (b) Bottom surface.

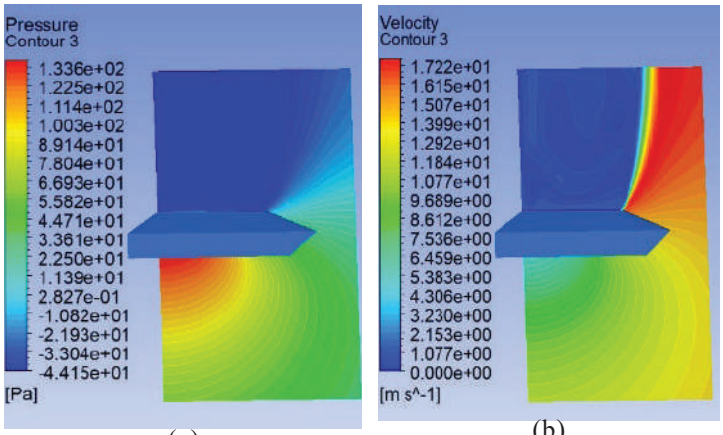

(a) (b)

Figure 15. Plot for the baseline delta wing at α = 35° and x/c =0.6. (a) Pressure contour; and (b) Velocity contour.

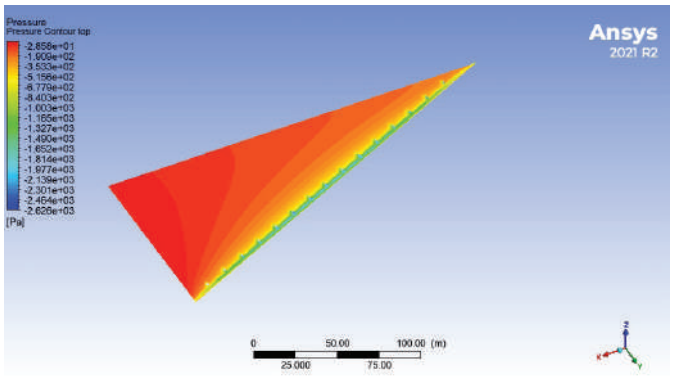

Figure 16. Pressure contour for the delta wing with case 2 on the top surface at α = 30°.

2 is marginal and does not seem to have much impact on the delta wing aerodynamics. For 30° and 35° angles of attack, as shown in Figures 12 and 13, respectively, the C_p curve for case 1 is flattened and shows highly reduced suction, and therefore the baseline delta wings tend to show stall behaviour. Case 3 proves to be more effective in delaying the flow separation. Therefore, the above results verified the increased operating

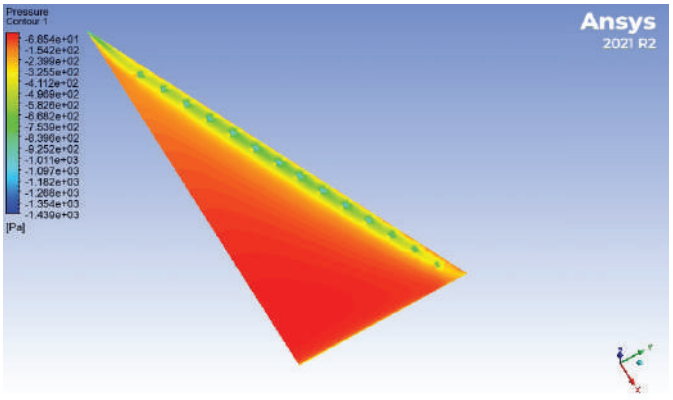

Figure 17. Pressure contour for the delta wing with case 3 on the top surface at α = 30°.

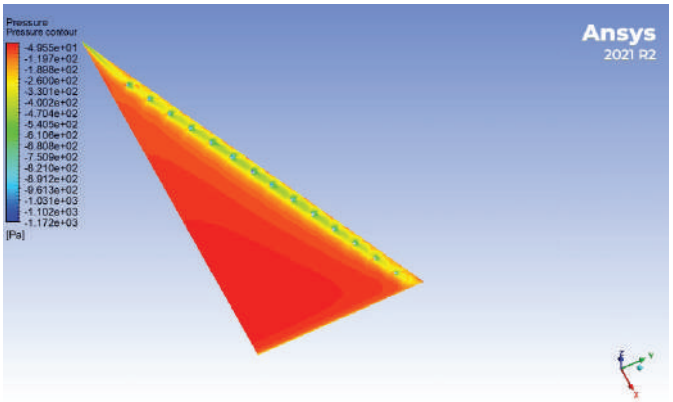

Figure 18. Pressure contour for the delta wing with case 4 on the top surface at α = 30°.

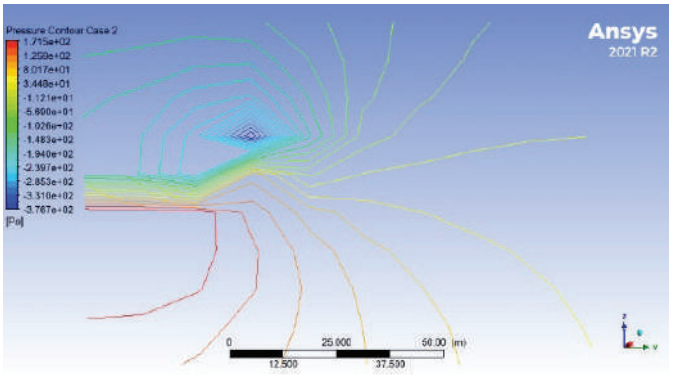

(a) Case 2

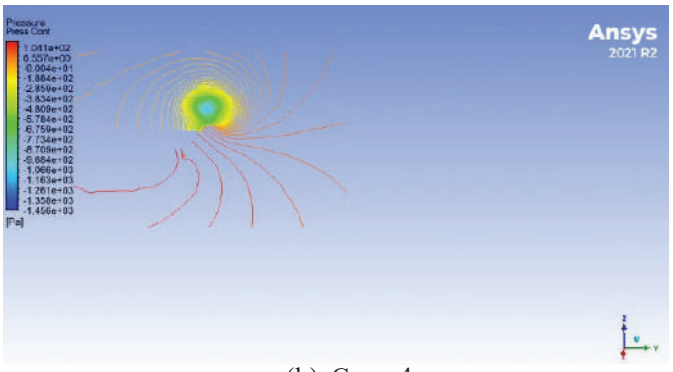

(b) Case 4

Figure 19. Pressure contour at α = 30°& x/c = 0.6.

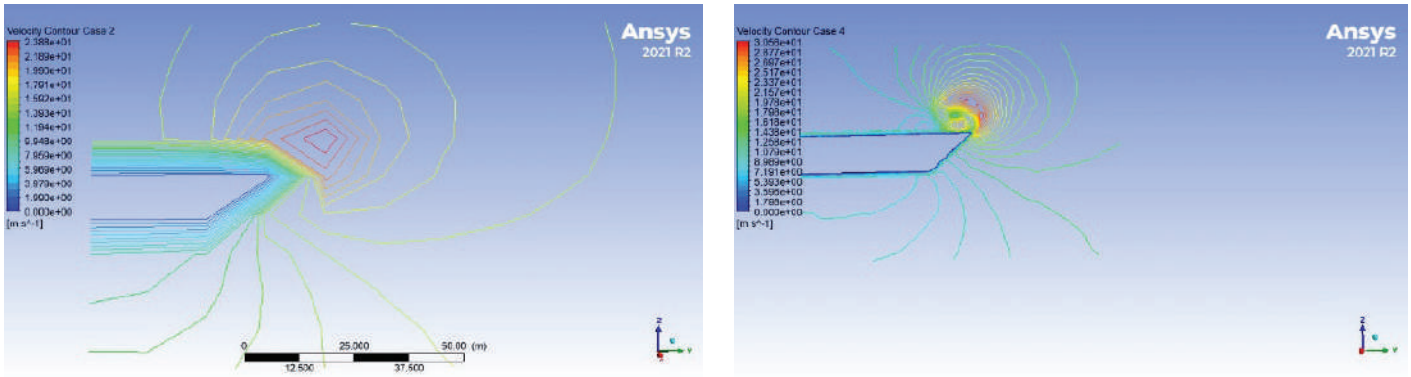

(a) Case 2 (b) Case 4

Figure 20. Velocity contour for the delta wing with case 2 at α = 30°& x/c = 0.6.

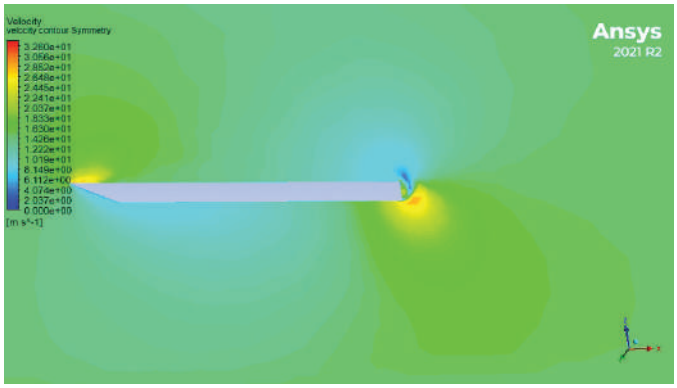

Figure 21. Velocity contour on the symmetry plane for the delta wing with case 3 at α = 30°.

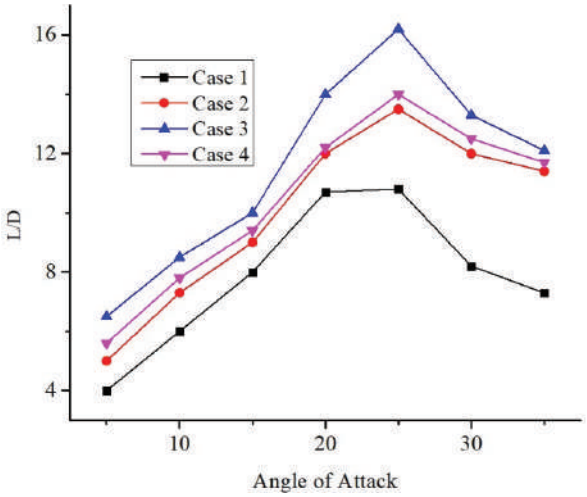

Figure 22. Comparison of L/D ratio versus angle of attack.

range of the angle of attack. The blowing phenomenon of controlling the flow seems to be effective. The blowing near the flow separation zone effectively increases the aerodynamic efficiency.

The pressure contour for the baseline delta wing on the top and bottom surface at α = 35° is shown in Fig. 14(a), 14(b), respectively. The peak pressure on the delta wing is located near the apex region and the bottom surface. The pressure contour plot and velocity plot for the baseline delta wing at α = 35° and x/c =0.6 are shown in Fig. 15(a) and 15(b), respectively. The pressure contour on the top surface at α = 30° for case 2, case 3 and case 4 are shown in Fig. 16, 17 and 18, respectively. The maximum peak suction pressure on the top surface can be observed for case 3. Maximum suction on the top surface will maximise the lift produced by the wing. Therefore, these results clearly depict the effectiveness of the active flow control technique for the case 3 delta wing. Figure 19(a,b) show the pressure contours for the delta wing with case 2, and case 4, respectively at α = 30°and x/c = 0.6. Also, Fig. 20(a,b) show the velocity contours for the delta wing with case 2, and case 4, respectively at α = 30°and x/c = 0.6. For the case 3 delta wing, the velocity contour plotted on the symmetry plane is shown in Fig. 21.

The lift-to-drag ratio (L/D) at various angles of attack was calculated for the baseline and the other blowing delta wing configurations. The plot comparison of L/D ratio vs. angle of attack is shown in Fig. 22. which clearly shows the effectiveness and the aerodynamic efficiency. The L/D ratio for a delta wing of case 3 proved to possess the highest aerodynamic efficiency.

4. CONCLUSIONS

The concept of blowing as a flow control technique has been applied to the delta wings. The blowing location was varied laterally on the suction surface of the delta wing. Three locations of blowing holes were identified to investigate the effect of blowing and its effect in delaying the vortex breakdown. The blowing configuration shown in case 3 proved superior to the other configurations in delaying the vortex breakdown. The artificial jet generated by blowing the fluid in the delta wing configuration of case 3 provides an adequate amount of momentum and hence energy to the vortex core. This transfer of energy from the jet to the vortex enables it to propagate downstream of the delta wing, and hence the phenomenon of vortex breakdown can be delayed. Moreover, the operating range of the angle of attack is further increased. Therefore, identifying the best location for blowing holes helps in delaying the vortex breakdown which certainly extends the angle of attack range as well as the aerodynamic efficiency of the wing.

REFERENCES

1. Chu, J. & Luckring, J.M. Experimental surface pressure data obtained on 65° delta wing across reynolds number and mach number ranges, NASA TM 4645, **1996**
2. Polhamus, E.C. Predictions of vortex-lift characteristics

by a leading edge suction analogy. *J. Aircr.* 1971, **8**, 193–199,
doi: 10.2514/3.44254
3. Polhamus, E.C. Charts for predicting the subsonic vortex-lift characteristics of arrow, delta and diamond wings; NASA TN D6243; NASA: Washington, DC, USA, 1971. Contract_Grant: 126-13-10-01
4. Mitchell, A.M.; Barberis, D. & Délery, J. Oscillation of vortex breakdown location and its control by tangential blowing. In Proceedings of the 29th AIAA, Fluid Dynamics Conference, Dallas, TX,USA, 22–26 June 1998; Volume 38, pp. 1–11.
doi: 10.2514/6.1998-2914.
5. Greenblatt, D.; Kastantin, Y.; Nayeri, C.N. & Paschereit, C.O. Delta-wing flow control using dielectric barrier discharge actuators. *AIAAJ.* 2008, **46**, 1554–1560.
doi:10.2514/1.33808.
6. Margalit, S.; Greenblatt, D.; Seifert, A. & Wygnanski, I. Delta wing stall and roll control using segmented piezoelectric fluidic actuators. *J. Aircr.*2005, **42**, 698–709.
doi: 10.2514/1.6904.
7. Roupassov, D.V.; Nikipelov, A.A.; Nudnova, M.M. & Starikovskii, A.Y. Flow separation control by plasma actuator with nanosecond pulsed-periodic discharge. *AIAAJ.*2009, **47**, 168–185.
doi: 10.2514/1.38113.
8. Nishihara, M.; Takashima, K.; Rich, J.W.; Adamovich, I.V. Mach 5 bow shock control by a nanosecond pulse surface dielectric barrier discharge. *Phys. Fluids,* 2011, **23**(6)*,* 066101.
doi: 10.1063/1.3599697.
9. Benard, N.; Zouzou, N.; Claverie, A.; Sotton, J. & Moreau, E. Optical visualization and electrical characterisation of fast-rising pulsed dielectric barrier discharge for airflow control applications. *J. Appl. Phys.* 2012, **111**(3)*,* 033303.
doi: 10.1063/1.3682568.
10. Zhao, G.Y.; Li, Y.H.; Hua, W.Z.; Liang, H.; Han, M.H. & Niu, Z.G. Experimental study of flow control on delta wings with different sweep angles using pulsed nanosecond DBD plasma actuators. *Proc. Inst. Mech. Eng. PartGJ. Aerosp. Eng.* 2015, **229**, 1966–1974.
doi: 10.1177/0954410014562630.
11. Yavuz, M.M. & Rockwell, D. Identification and control of three-dimensional separation on low swept delta wing. *AIAAJ.* 2006, **44**, 2805–2811.
doi: 10.2514/1.24756.
12. Yaniktepe, B. & Rockwell, D. Flow structure on diamond and lambda planforms: Trailing-edge region. *AIAAJ.* 2005, **43**, 1490–1500.
doi: 10.2514/1.7618.
13. Ol, M.V. & Gharib, M. Leading-edge vortex structure of nonslender delta wings at low Reynolds number. *AIAAJ.*2003, **41**, 16–26.
doi: 10.2514/2.1930.
14. Taylor, G.S. & Gursul, I. Buffeting flows over a low-sweep delta wing. *AIAAJ.*2004, **42**, 1737–1745.
doi: 10.2514/1.5391.
15. Chen, L.; Wang, J.; Zuo, L.X. & Feng, L.H. Influence of Reynolds number on vortex flow over a non-slender delta wing. *AIAAJ.*2010, **48**, 2831–2839.
doi: 10.2514/1.J050246
16. Sahin, B.; Yayla, S.; Canpolat, C. & Akilli, H. Flow structure over the yawed non slender diamond wing. *Aerosp. Sci.Technol.* 2012, **23**, 108–119.
doi: 10.1016/j.ast.2011.06.008.
17. Gursul, I.; Wang, Z. & Vardaki, E. Review of flow control mechanisms of leading-edge vortices. *Prog. Aerosp.Sci.,* 2007, **43**, 246–270.
doi:10.1016/j.paerosci.2007.08.001.
18. F. Renac, F.; Barberis, D. & Molton. P. Control of vortical flow over a rounded leading-edge delta wing. *AIAAJ.,* 2005, **43**, 1409–1418.
doi:10.2514/1.7265.
19. Hong, J.S.; Çelik, Z.Z. & Roberts, L. Effects of leading-edge lateral blowing on delta wing aerodynamics. *AIAAJ.,* 1996, **34**, 2471–2478.
doi:10.2514/3.13426.
20. Wood, N.J. & Roberts, L. Control of vortical lift on delta wings by tangential leading-edge blowing. *J.Aircr.,* 1988, **25**, 236–243.
doi:10.2514/3.45583.
21. Greenwell, D.I. & Wood, N.J. Roll moment characteristics of asymmetric tangential leading-edge blowing on a delta wing. *J. Aircr.,* 1994, **31**, 161–168.
doi:10.2514/3.46469.
22. Gu. W.; Robinson, O. & Rockwell, D. Control of Vortices on a delta wing by leading-edge injection. *AIAAJ.,* 1993, **31**, 1177–1186.
doi:10.2514/3.11749
23. Williams, N.M.; Wang, Z. & Gursul, I. Active flow control on a non-slender delta wing. *J.Aircr.,* 2008, **45**, 2100–2110.
doi:10.2514/1.37486.
24. Cui, Y.D.; Lim, T.T. & Tsai, H.M. Control of vortex breakdown over a delta wing using forebody slot blowing. *AIAAJ.,* 2007, **45**, 110–117,
doi:10.2514/1.22575
25. Jiang, P.; Wang, Z. & Gursul, I. Effects of unsteady trailing-edge blowing on delta wing aerodynamics. *J.Aircr.,* 2010, **47**, 591–602.
doi:10.2514/1.45890.
26. Johari, H.; Olinger, D.J. & Fitzpatrick, K.C. Delta wing vortex control via recessed angled spanwise blowing. *J. Aircr.,* 1995, **32**, 804–810.
doi:10.2514/3.46794.
27. Lamar, J.E. Special course on fundamental of fighter aircraft design. *AGARD Rep.,* 1988, **740**, 9.
28. Rao, D.M. & Campbell, J.F. Vortical flow management techniques, Prog. *Aerosp. Sci.,* 1987, **24**, 173–224.
doi:10.1016/0376-0421(87)90007-8.
29. Smith, A.; Balogun, H.; Khan, M.; Aji, C. & Salehian, S. Characterization of the flow field of slender and non-slender delta wings using volumetric PIV, AIAA 2022-1195. In AIAASCITECH2022Forum; AIAA: Reston, VA, USA, 2022.
doi:10.2514/6.2022-1195

30. Sedlacek, D. & Breitsamter, C. Aerodynamic Characteristics and topology of interfering vortex systems at hybrid delta wings, AIAA 2022-0026. In *AIAASCITECHForum*; AIAA: Reston, VA, USA, 2022, doi:10.2514/6.2022-0026
31. Balogun, H.; Smith, A.; Khan, M.J. & Aji, C.A., Characterization of the flow field of slender delta wings with trailing edge jets using volumetric PIV, AIAA 2023-2300. In *AIAASCITECHForum*; AIAA: Reston, VA, USA, 2023. doi: 10.2514/6.2022-1195
32. Al-Garni Ahmad, Z.; Saeed, F. & Al-Garni Abdullah, M. Experimental and numerical investigation of 65° delta and 65/40° double-delta wings. *J.Aircr.,* 2008, **45**, 71–76. doi: 10.2514/1.20243.
33. Wentz, W.H. & Kohlman, D.L. Vortex breakdown on slender sharp-edged wings. *J.Aircr.,* 1971, **8**, 156–161. doi: 10.2514/3.44247
34. Cummings, R.M.; Morton, S.A. & McDaniel, D.R. Experiences in accurately predicting time-dependent flows. *Prog. Aerosp. Sci.,* 2008, **44**, 241–257. doi:10.1016/j.paerosci.2008.01.001
35. Allan, M. A CFD investigation of wind tunnel interference on delta wing aerodynamics. Ph.D. Thesis, University of Glasgow, Glasgow, Scotland, UK, 2002.
36. Ramakrishna, M.S.K.C. & Venkatesh, B. Influence of leading edge shapes on vortex behaviour of delta wing. *IOP Conf. Ser. J. Phys.,* 2019, **1276**, 012008. doi:10.1088/1742-6596/1276/1/012008.

CONTRIBUTORS

Mr Sugandh Gupta is pursuing PhD from Punjab Engineering College, Chandigarh, India. Presently, he is working as an Assistant Professor in the Department of Aerospace Engineering at Chandigarh University, Punjab, India. His areas of specialisation are: Experimental aerodynamics, computational fluid dynamics and flow control techniques.
In the current study, he carried out the simulation work along with the interpretation and analysis of the results.

Dr. Sanjeev Kumar obtained his PhD from Thapar Institute of Engineering and Technology. Presently, he is working as a Professor and Head in the Department of Mechanical Engineering at Punjab Engineering College, Chandigarh, India. His areas of specialisation are: Advanced manufacturing techniques and material science.
In the current study, he has assisted in reviewing the progress of work and provided several valuable suggestions.

Dr Rakesh Kumar obtained his PhD in Aerospace Engineering from IIT, Kanpur, India. Presently, he is working as a Professor and Head in the Department of Aerospace Engineering, at Punjab Engineering College, Chandigarh, India. His areas of interest are: Flight mechanics, aerodynamics and artificial neural networks.
In the current study, he has given the idea, reviewed the results and provided several valuable inputs.